Journal of The Electrochemical Society, 2024 **171** 030508

Impact of Processing Methodology on the Performance of Hybrid Sulfide-Polymer Solid State Electrolytes for Lithium Metal Batteries

Priyadarshini Mirmira,[=] Claire Fuschi,[=] Zoe Umlauf, Peiyuan Ma, Emily S. Doyle, Minh Canh Vu, and Chibueze V. Amanchukwu[*,z]

Pritzker School of Molecular Engineering, University of Chicago, Chicago Illinois 60637, United States of America

Hybrid sulfide-polymer composite electrolytes are promising candidates to enable lithium metal batteries because of their high ionic conductivity and flexibility. These composite materials are primarily prepared through solution casting methods to obtain a homogenous distribution of polymer within the inorganic. However, little is known about the influence of the morphology of the polymer and the inorganic on the ionic conductivity and electrochemical behavior of these hybrid systems. In this study, we assess the impact of processing methodology, either solution processing or solvent-free ball milling, on overall performance of hybrid electrolytes containing amorphous Li_3PS_4 (LPS) and non-reactive polyethylene (PE). We demonstrate that using even non-polar, non-reactive solvents can alter the LPS crystalline structure, leading to a lower ionic conductivity. Additionally, we show that ball milling leads to a non-homogenous distribution of polymer within the inorganic, which leads to a higher ionic conductivity than samples processed via solution casting. Our work demonstrates that the morphology of the polymer and the sulfide plays a key role in the ionic conductivity and subsequent electrochemical stability of these hybrid electrolytes.

 [DOI: 10.1149/1945-7111/ad2d3e]

Manuscript submitted November 2, 2023; revised manuscript received February 14, 2024. Published March 7, 2024.

Supplementary material for this article is available online

Lithium metal batteries are currently one of the most promising battery chemistries to address large-scale energy storage challenges such as the electrification of transport.[1] However, conventional carbonate-based liquid electrolytes are unsuitable for lithium-metal anodes because they are volatile, flammable, and enable lithium dendrite formation, leading to cell failure.[2] One avenue to overcome these challenges is the use of solid-state electrolytes, which can be nonvolatile, non-flammable, and have conductivities similar to or higher than liquid electrolytes.[3,4] State-of-the-art sulfide-type inorganic electrolytes have high room temperature conductivity but are plagued by poor mechanical properties, causing them to fracture during cycling with Li-metal.[5,6] On the other hand, polymer electrolytes are flexible and can withstand the volume changes that occur during battery cycling, but suffer from poor ionic conductivities.[7] Thus, polymers can be added to sulfide-type inorganic electrolytes to develop hybrid electrolytes.[8] These hybrid electrolytes leverage the high Li-conductivity of the sulfide and the advantageous mechanical properties of the polymer.

In the hybrid electrolyte literature, the state-of-the-art polymer electrolyte poly(ethylene oxide) (PEO) is combined with sulfide-type inorganic electrolytes to improve cycle life.[9–11] Recently, our group reported on the development of Li_3PS_4 (LPS)-based hybrid electrolytes that leverage non-conductive, non-reactive polyethylene (PE) as the polymer component.[12] We observed that hybrids using PE had a higher conductivity than those made with PEO, primarily due to the degradation of both LPS and PEO that occurs upon synthesis of the LPS-PEO hybrid electrolyte.[12,13] Additionally, we discovered that PEO provides an alternative, competing pathway for ion-transport which ultimately lowers the conductivity of the overall hybrid. We were able to overcome these challenges by substituting PEO with non-polar, non-reactive PE. The hybrids presented in this previous work were synthesized via ball-milling to eliminate any potential effects from solvent processing as sulfide-type inorganics are known to be particularly sensitive to solvent choice.[14–16] However, the optimization of solution-based synthetic methods is necessary to scale these electrolytes. Therefore, a systematic investigation of the role of processing on sulfide-polymer hybrid electrolytes is needed.

Several studies in the polymer-sulfide literature employ solution processing and annealing to prepare electrolyte films.[8–10,17,18] It is generally assumed that solution processing is advantageous because of low cost and the production of a good polymer-ceramic interface due to a uniform distribution of polymer-in-ceramic or ceramic-in-polymer.[19–21] However, this method has several drawbacks such as solvent complexation with the sulfide, leading to a lower conductivity than dry-processed electrolytes.[14,16,22] Previous work in the literature has demonstrated that sulfide-type electrolytes are highly reactive and degrade in the presence of common organic solvents such as acetonitrile and dimethylformamide (DMF).[14,16] Additional work has shown that this degradation can be minimized by using nonpolar organic solvents such as toluene[14] and ethyl acetate,[22] demonstrating that solvent choice is a non-trivial consideration in the processing of hybrid electrolytes.

While solvent selection has been widely studied in sulfide-based composite electrolytes, the relationship between polymer distribution and electrolyte performance is not completely understood. Studies by Goodenough et al.,[19] and Hatzell et al.,[23] have demonstrated that in hybrids utilizing oxide-type inorganics with PEO, solution processing leads to more uniform distribution of polymer throughout the inorganic. Only a few studies have pursued a ball milling approach to synthesizing sulfide-polymer composites,[24,25] but the distribution of the polymer and inorganic was not investigated. In this study, we compare the effects of two fabrication methods, ball milling and solution processing, on overall performance of hybrid sulfide-polymer composite electrolytes. Using scanning electron microscopy (SEM) with electron dispersion X-ray spectroscopy (EDS), we show that the microstructure of the electrolyte differs based on processing methodology, with the solution-processed samples displaying a more homogenous distribution of polymer within the LPS matrix. However, using electrochemical impedance spectroscopy (EIS), we show that the overall conductivity of the solution processed samples is much lower than the ball-milled counterparts. The low conductivity of the solution processed samples leads to higher overpotentials during Li||Li symmetric cell cycling. Our findings demonstrate that the performance of sulfide-polymer hybrids is greatly dependent on the

[=]Equal contribution.
*Electrochemical Society Member.
[z]E-mail: chibueze@uchicago.edu

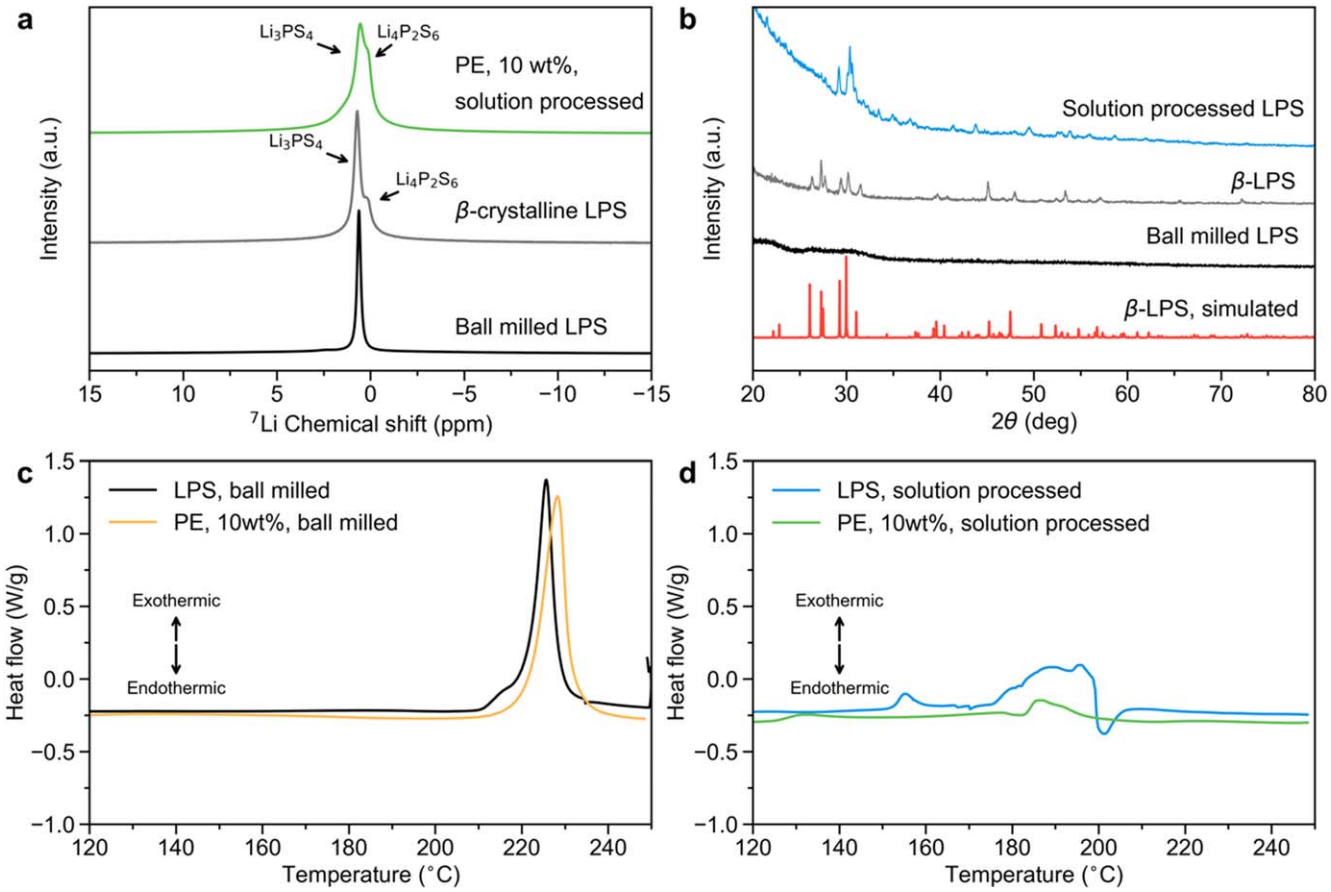

Figure 1. Understanding Li_3PS_4 (LPS) phase changes during solution processing. (a) ^{7}Li magic angle spinning (MAS) NMR of ball milled LPS, β-crystalline LPS, and a solution processed 10 wt% polyethylene (PE) hybrid. (b) XRD patterns of amorphous, β-crystalline, and solution processed LPS, and simulated β-crystalline LPS obtained from the Materials Project for LPS (mp-985583).[26] Differential scanning calorimetry (DSC) scans of (c) ball milled LPS and a ball milled 10 wt% PE hybrid, and (d) solution processed LPS and a solution processed 10 wt% PE hybrid. All ball milled data from subfigures (a)–(c) have been reproduced with permission from *ACS Appl. Energy Mater.* 2022, 5 (7), 8900–8912.

method of processing the electrolyte (irrespective of the chosen polymer binder), and that the conventional slurry-casting method to prepare sulfide-type hybrids may lead to a decrease in overall hybrid performance.

Results and Discussion

Impact of solution processing on Li_3PS_4 phase stability.— Solution processing of hybrid sulfide-polymer electrolytes is a common method of synthesizing these materials in the literature.[14] In particular, solvent compatibility with the sulfide inorganic plays a large role in the overall performance of the hybrid electrolyte. Chen et al.[14] systematically studied the solvent compatibility of a $Li_3P_7S_{11}$ sulfide-type electrolyte with polar and non-polar solvents and discovered that polar solvents, such as acetonitrile and dimethylformamide, degrade the $Li_3P_7S_{11}$ crystalline structure. Additionally, they also showed that processing hybrid electrolytes in non-polar solvents such as toluene or xylene preserved the $Li_3P_7S_{11}$ crystal structure, leading to a better overall electrochemical performance than samples processed in polar solvents.

Additional studies by Sedlmaier et al.[27] show that these same polar solvents can lead to the formation of polysulfide species in amorphous Li_3PS_4 (LPS). Therefore, using this precedent, we solution processed our PE-LPS hybrid electrolytes in toluene for two principal reasons: (1) toluene is a non-polar solvent and therefore should not interact with or degrade the amorphous LPS into polysulfide species, and (2) toluene is one of the few solvents known to dissolve PE at high temperatures such as 90 °C. After mixing LPS and PE in toluene at 90 °C, the samples were vacuum dried, also at 90 °C, to remove residual solvent. Removal of toluene was confirmed by solution state ^{1}H NMR (Fig. S1) of a 10 wt% PE hybrid. No proton peaks attributable to toluene can be observed in these spectra. To confirm the chemical stability of LPS after solution processing, ^{7}Li solid state magic-angle spinning nuclear magnetic resonance (ssNMR) spectroscopy was employed (Fig. 1a). Ball milled, amorphous LPS should display one, sharp peak around 0.5 ppm with a full-width-half-maximum (FWHM) of 43 Hz. The same was expected for the solution processed 10 wt% PE hybrid. However, the hybrid showed two peaks, resonating at 0.55 ppm and 0.15 ppm, with a FWHM of 114 Hz and 72 Hz, respectively. No peaks corresponding to unreacted Li_2S precursor (~2.3 ppm) were observed in either the pristine ball milled LPS or the 10 wt% PE hybrid. To check if these two peaks could be the result of crystallization of amorphous LPS, β-crystalline LPS was synthesized and the resulting ^{7}Li ssNMR spectrum was compared (Fig. 1a). β-crystalline LPS also exhibits two peaks, one at 0.7 ppm and the other at 0.12 ppm, with a FWHM of 104 Hz and 77 Hz, respectively.[28] Given the similarity of the linewidths and peak positions between the β-crystalline LPS and the solution processed 10 wt% PE hybrid, we hypothesized that the solution processing method might have induced a degree of crystallinity in the amorphous LPS, as has been reported for hybrids processed in polar solvents.[16,17,22,27] Given that toluene is nonpolar, we anticipate that this induced crystallinity may come from the heating step to remove the solvent, as crystalline forms of LPS require high temperatures (>100 °C) to access.[16]

To confirm the potential crystallization of amorphous LPS, a control sample was synthesized, where amorphous LPS without PE

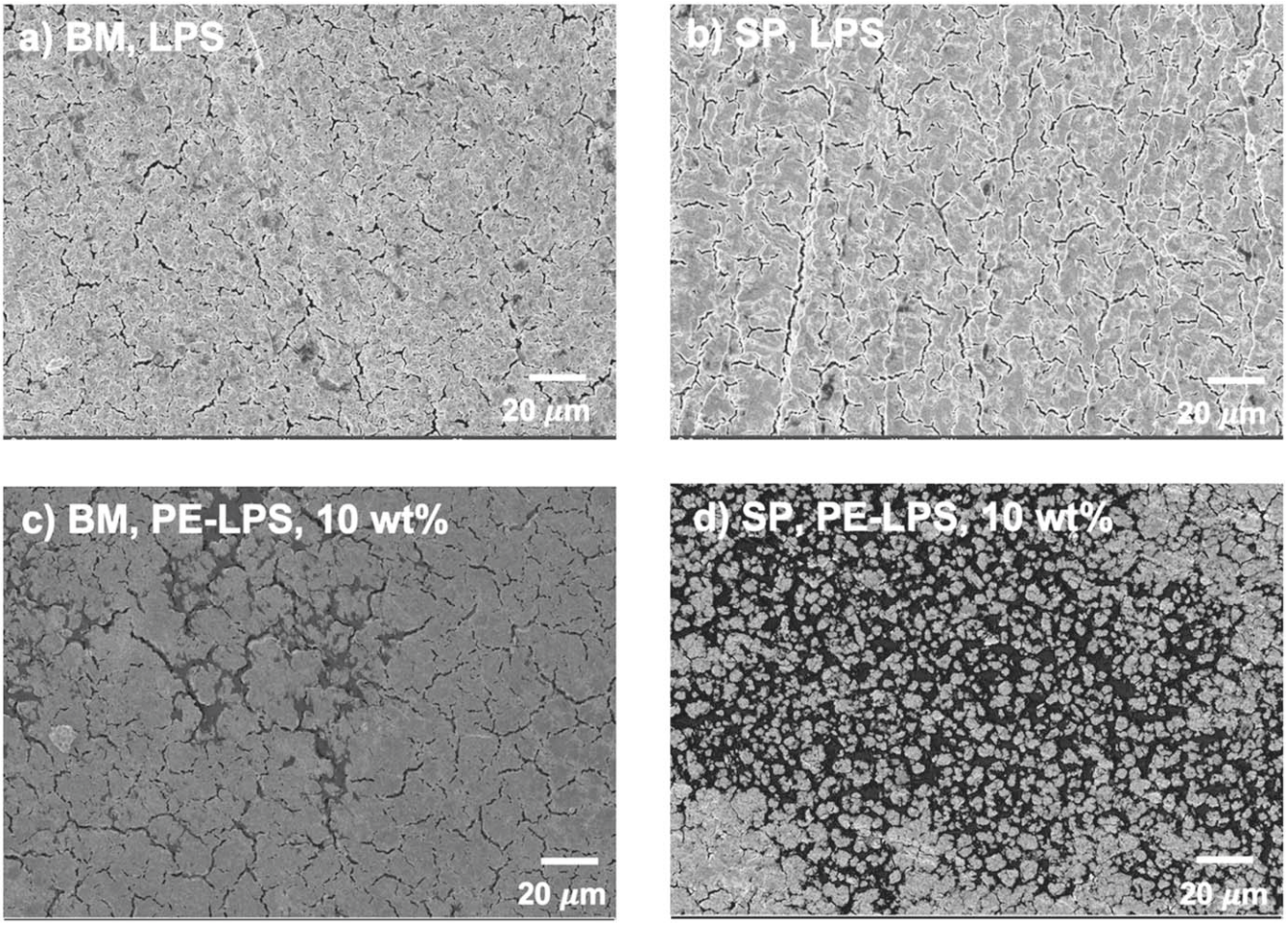

Figure 2. Probing surface morphology through SEM. SEM images of electrolyte pellet surfaces composed of (a) ball milled (BM) pure LPS, (b) solution processed (SP) pure LPS, (c) ball milled PE-LPS at 10 wt%, and (d) solution processed PE-LPS at 10 wt%.

was suspended in toluene, and then vacuum dried at 90 °C. X-ray diffraction (XRD) of the solution processed LPS, amorphous LPS, and β-crystalline LPS was performed (Fig. 1b) to understand the impact of processing in a non-polar solvent on amorphous LPS crystallization. Amorphous LPS exhibits large "humps" around 20° and 30° (2θ), similar to previous reports for this material.[17,29] The β-crystalline LPS shows several peaks between 20° and 30° and additional minor peaks between 50° and 60°, comparable to several literature reports.[30–32] Interestingly, the solution processed, amorphous LPS no longer has broad "humps," and instead displays several peaks. Of particular note in the solution processed sample are the peaks at 29° and 33° which appear to align with the set of three peaks at 29°, 31°, and 33° on the β-crystalline LPS pattern. Although from the XRD patterns, it does not appear that the solution processed LPS becomes fully β-crystalline, the presence of these peaks indicates that the phase of the inorganic in a solution processed polymer hybrid has changed.

To investigate the crystallization behavior of LPS processed in toluene and the polymer hybrids, differential scanning calorimetry (DSC) was employed (Figs. 1c and 1d). As shown in Fig. 1c, pure ball milled LPS exhibits a characteristic exothermic peak around 225 °C attributed to crystallization.[33,34] This peak is also seen in the ball milled PE hybrid, however the peak is significantly depressed in the solution processed LPS and solution processed PE hybrid (Fig. 1d). To quantify the approximate percent crystallinity in the solution processed LPS and the solution processed PE hybrid, the crystallization peaks were integrated and compared with the ball milled counterparts. The integrations of ball milled pure LPS (10.28 J g^{-1}) and ball milled PE hybrid (11.31 J g^{-1}) are approximately the same, and both are greater than the solution processed samples. Integration shows that the crystallization in the solution processed LPS is suppressed to 7.02 J g^{-1} and the subsequent PE hybrid to 4.86 J g^{-1}. This would correspond to roughly 32% crystallinity for the solution processed LPS and 57% crystallinity for the PE hybrid. This suggests that solution processing with toluene alters the structure of the initially amorphous LPS. Given that amorphous LPS is the most conductive form of LPS,[35] the induced crystallinity will have an overall negative impact on the conductivity of the LPS-PE electrolyte, and this will be discussed later.

Effect of processing on hybrid electrolyte microstructure.—The method of processing the hybrid sulfide-polymer electrolyte can have a large impact on the microstructure, or the distribution of the polymer and sulfide within the electrolyte.[19,23] Therefore, the surface morphology of the ball milled and solution processed hybrids was investigated using SEM (Fig. 2). The morphology of the control LPS samples did not appear to change between the two processing methods (Figs. 2a–2b), indicating that the processing in toluene does not alter the size of the LPS particles. However, there is a clear distinction between the two methods for each of the polyethylene-containing hybrids. The solution processed, 10 wt% PE (Fig. 2d) hybrid materials exhibited a more homogenous morphology, with the polymer distributed mostly evenly throughout the surface of the pellet. By contrast, the ball milled, 10 wt% PE (Fig. 2c) sample displayed dark chunks of polymer that appear to be randomly dispersed throughout the inorganic. This trend does not seem to be dependent on the polymer identity as Fig. S2 shows SEM images of ball milled and solution processed 10 wt%, PEO hybrids. Similarly,

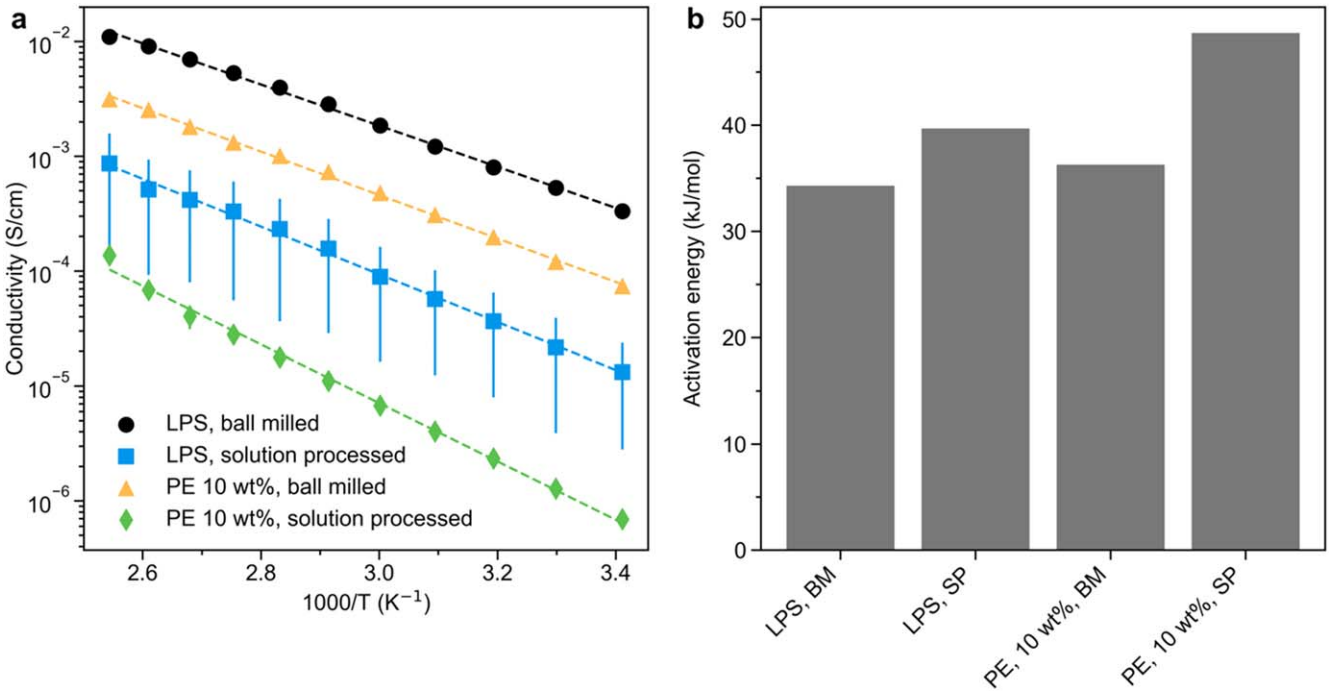

Figure 3. Understanding the effect of processing on ionic conductivity and activation energy. Ionic conductivity of (a) ball milled (BM) and solution processed (SP) LPS and 10 wt% PE hybrid electrolytes, and (b) activation energy for hybrid electrolytes obtained from Arrhenius fitting. Error bars are present for all data in subfigures (a) and (b). Ball milled data in subfigures (a) and (b) have been reproduced with permission from *ACS Appl. Energy Mater.* 2022, *5* (7), 8900–8912.

in the ball milled PEO hybrid, there appears to be large, dark chunks of polymer, randomly dispersed throughout the inorganic. Additionally, in the solution processed PEO hybrid, the polymer also seems to be evenly dispersed throughout the inorganic, indicating that processing in solution affords a more homogenous distribution of polymer within the inorganic than ball milling. To confirm our assignment of the polymeric versus inorganic regions, a new 10 wt% PE solution processed hybrid was synthesized and SEM with energy-dispersive X-ray spectroscopy (EDS) images were taken (Fig. S3). Although the resolution of this image is lower than the images shown in Fig. 2, the areas of polymer and the inorganic are still clear. The sulfur and phosphorus elemental mapping show dark regions which overlap with the carbon mapping, confirming that the polymer is homogeneously distributed throughout the inorganic in this area.

One striking observation contrasting the ball milled (Fig. 2c) and solution processed PE hybrid (Fig. 2d) is that the way in which the polymer interacts with the LPS appears to be different. Figure S2 displays higher magnification images of the ball milled and solution processed PE hybrids. In the ball milled PE sample, the polymer seems to fill the cracks of the LPS pellet, or at the very least, bridge the gap between the LPS particles. By contrast, in the solution processed PE sample, the polymer appears to physically separate the particles of the LPS, and it seems that the LPS is sitting inside the matrix of the PE. In the case of the ball milled PEO and solution processed PEO (Fig. S2) samples, there does not seem to be as stark of a separation of several LPS particles by the polymer. Yet in both ball milled PE and PEO polymer hybrids, the LPS phase is more contiguous than in the solution processed samples. The electrochemical implications of the polymer distribution within the inorganic will be discussed later.

Effect of processing on hybrid electrolyte conductivity and activation energy.—To understand the effect of processing on Li-ion migration performance, temperature-dependent ionic conductivity was measured, and the results for the ball milled and solution cast hybrids are shown in Fig. 3a. All conductivity curves were fit according to the Arrhenius equation:

$$\sigma = A \exp\left(\frac{-E_a}{RT}\right) \quad [1]$$

where σ is the ionic conductivity, E_a is the activation energy, T is the temperature, and R is the ideal gas constant (8.314 kJ mol^{-1}). Arrhenius-type dependence, typically reported for inorganics,[36] was found for all samples in both solution cast and ball milled families, and the computed activation energies can be found in Fig. 3b.

We have previously reported the ionic conductivity of the ball milled PE hybrid, and demonstrated that PE-based hybrids outperform PEO-based hybrids by a factor of 2 or greater, further motivating the choice to use PE for this study.[12] However, the method of processing these hybrids (regardless of polymer identity) plays a significant role in determining the ionic conductivity. As demonstrated by Fig. 3a, the solution processed 10 wt% PE hybrid has a conductivity of 6.9×10^{-7} S cm^{-1} at 20 °C. This is approximately three orders of magnitude lower than the ball milled LPS and almost two orders of magnitude lower than the ball milled PE hybrid. This observation has been reported for other non-conductive polymers such as styrene-butadiene rubber (SBR). Kanno et al.[20] also observed that a dry-processed (mortar and pestle) hybrid composed of $Li_{3.25}Ge_{0.25}P_{0.75}S_4$ (LGPS) and SBR binder led to a higher ionic conductivity than a slurry-cast analogue. The authors posited that the homogenous distribution of the SBR in the slurry-cast hybrid may be the cause of this reduction in conductivity, but the concentration of polymer (4 vol%) appeared to be too low to see a distinction in their SEM images. A physical separation of the LPS particles by a non-conductive polymer was not reported in their study.

We discussed previously that toluene-processing imparts a degree of crystallinity on the formerly amorphous LPS. It has been well-reported that the crystalline phase of LPS greatly affects the conductivity, with the amorphous form being the most conductive, and the β, α, and γ-crystalline forms having lower conductivity, respectively.[37] β-crystalline LPS reportedly has a conductivity of approximately 1.6×10^{-4} S cm^{-1},[17,38] which is about an order of magnitude greater than the solution processed LPS (1.3×10^{-5} S cm^{-1}). As shown by the

XRD patterns in Fig. 1b, while the solution processed LPS has a degree of crystallinity, it is not fully β-crystalline, which may account for the difference in conductivity. Given this, it must be acknowledged that the solution processed PE hybrid contains an inorganic that has lower conductivity than its ball milled counterpart. However, the reduction in LPS conductivity alone is insufficient to fully account for the large difference in conductivity between the ball milled and solution processed hybrid electrolytes.

In addition to the conductivity, the activation energies for Li^+-transport are quite different between the ball milled and solution processed hybrid electrolytes (Fig. 3b). The ball milled, amorphous LPS has an activation energy of approximately 34 kJ mol^{-1}, comparable to several literature reports for this material.[16,31] Comparably, the ball milled PE hybrid has an activation energy of about 36 kJ mol^{-1}, approximately the same as the pure inorganic. By contrast, the solution processed samples seem to exhibit a higher activation energy than their ball milled counterparts. The solution processed LPS has an activation energy of about 40 kJ mol^{-1}, which is higher than the amorphous LPS but not too dissimilar from β-crystalline LPS, reported to be about 38 kJ mol^{-1}.[39] Therefore, we attribute the higher activation energy in the solution processed LPS to the induced crystallinity from solution processing, which is consistent with the lower conductivity.[28,37] However, there appears to be a large jump in the activation energy when moving from the solution processed, pristine LPS to the solution processed PE hybrid. With only the addition of 10 wt% PE, the activation energy jumps from 40 kJ mol^{-1} to 48 kJ mol^{-1}, more than 10 kJ mol^{-1} greater than that of the ball milled PE analogue. Therefore, it is clearly more difficult for ions to transport through the solution processed hybrid than even the solution processed LPS control.

From literature reports, Li-ions move through β-crystalline LPS by "hopping" from one interstitial vacancy in the crystalline lattice to another.[40] The tetrahedral arrangement of the PS_4^{3-} blocks gives rise to faster lithium transport in the β-crystalline phase as compared to other crystalline phases.[28,37] Therefore, an increase in the activation energy for lithium transport, moving from inorganic to hybrid, indicates that the polymer may be preventing lithium from accessing the interstitial vacancies in the PS_4^{3-} lattice. Using insights gained from the SEM images shown in Fig. 2, we expect that the distribution of the polyethylene within the inorganic is responsible for the lower conductivity, and subsequently, the greater activation energy when comparing the ball milled and solution cast composites. Figure 2d showed not only a more homogenous distribution of the PE in the solution processed sample compared to the ball milled sample, but also an active separation of the particles of LPS within the hybrid caused by PE. Because ions cannot pass through the PE, the separation of the LPS particles ensures that there are fewer contiguous pathways of conduction through the LPS, leading to a greater activation energy.

To check how the conductivity of our solution processed PE hybrid compares to the literature, we have plotted the hybrid conductivity as a fraction of the inorganic conductivity for our work and other studies (Fig. S4) by Wang et al.,[41] Kanno et al.,[20] and Sedlmaier et al.[27] These studies all utilize a non-conductive polymer binder and a thiophosphate-type inorganic electrolyte and synthesize their electrolytes via solution processing. We observe that our solution processed PE hybrid can only maintain approximately 5% of the inorganic conductivity, while other reports demonstrate a much greater retention of the total conductivity (>20%). While it can be difficult to compare the electrolytes considering the different properties of each polymer component (e.g. PE vs styrene butadiene rubber (SBR)), we anticipate that the inorganic-polymer distribution is largely responsible for this difference. Most studies purport that polymers such as poly(vinylidene fluoride) (PvDF) and SBR are "good binders" for these sulfide inorganic electrolytes because they can enable flexible, thin films.[15,27,42] However, the definition of a "good binder" in these electrolytes has not been fully defined. Although our PE-based electrolyte pellets are thick (~0.2 mm), as will be discussed later, the cycling performance against Li-metal is significantly improved in comparison to the pristine inorganic.[12] We expect that although the distribution of the PE in our hybrid electrolytes leads to low conductivity, the conductivity alone does not govern cycling behavior. A detailed study of the relationship between inorganic-polymer distribution and mechanical properties is greatly needed to elucidate this phenomenon.

Conversely, the inhomogeneous distribution of PE in the ball milled sample (Fig. 2c) ensures that LPS pathways of ion-conduction are not as inhibited by the insulating polymer as in the solution processed sample. As a result, the conductivity is higher than that of the solution processed sample and the activation energy of the ball milled hybrid is similar to the pristine inorganic. This relationship between conductivity and distribution seems to be agnostic of the polymer. To check the generalizability of this observation, ball milled and solution processed PEO hybrids (also 10 wt% polymer) were fabricated. The conductivity of these hybrids (Fig. S5) was measured, and SEM images were taken (Fig. S2). Like the PE samples, the conductivity of the ball milled PEO sample is slightly higher than that of its solution processed counterpart. However, unlike the solution processed PE, no physical separation of the LPS particles is observed in the solution processed PEO sample. Although the PEO appears to cover more surface area in the solution processed sample than the ball milled sample, the polymer appears to fill the cracks between the LPS particles as opposed to separating the particles. Additionally, unlike PE, PEO can support ion conduction. Our previous work demonstrated that lithium polysulfide species form as a result of the reaction between PEO and LPS.[12] These polysulfide species can dissolve in ether-based electrolytes, like PEO, and provide a pathway of lithium conduction through the polymer.[43] This could explain why the conductivity of the solution processed PEO hybrid (1.59×10^{-5} S cm^{-1}), although lower, is closer to that of the ball milled version (1.72×10^{-5} S cm^{-1}).

The differences in the PE and PEO samples demonstrate that the polymer distribution within the inorganic plays a large role in the conductivity of the sulfide-polymer hybrid. This has been shown quite extensively for oxide-based composite materials (e.g. $Li_3La_7Zr_2O_{12}$ or LLZO), but the relationship is more complicated for sulfides. In LLZO-based systems, a conductive polymer (such as PEO) usually provides the main mode for Li-ion transport,[44,45] and the goal is to maximize the number of continuous pathways for ion transport through the polymer.[19] However, in sulfide-based systems, because the inorganic has a higher conductivity than conductive polymers, the goal should be to optimize pathways for transport through the sulfide. Additionally, because sulfides are more reactive than LLZO,[46] the use of a non-reactive polymer is important to preserving the chemical stability of the sulfide, and consequently the overall conductivity.[12]

Therefore, it seems that utilizing a non-conductive polymer with an inhomogeneous distribution, usually afforded by ball milling, is more advantageous than a slurry casting approach.

Influence of processing on electrochemical performance of hybrid electrolytes.—The electrochemical performance of the solution processed and ball milled hybrids was evaluated. Symmetric Li || Li half cells were fabricated, and long-term cycling measurements were conducted at 60 °C with a current density of 0.05 mA cm^{-2} to a capacity of 0.05 mAh cm^{-2} (Fig. 4). This current density was chosen because it was the only current density that all of the samples (ball milled and solution processed) could withstand without shorting too quickly (Fig. S6).[12] The critical current density of LPS does not appear to be significantly impacted by the introduction of PE. The maximum current density that all electrolytes can stably handle is 0.1 mA cm^{-2} to a capacity of 0.1 mAh cm^{-2}. All electrolytes either shorted completely at current densities above 0.25 mA cm^{-2} or could only cycle for < 5 cycles.

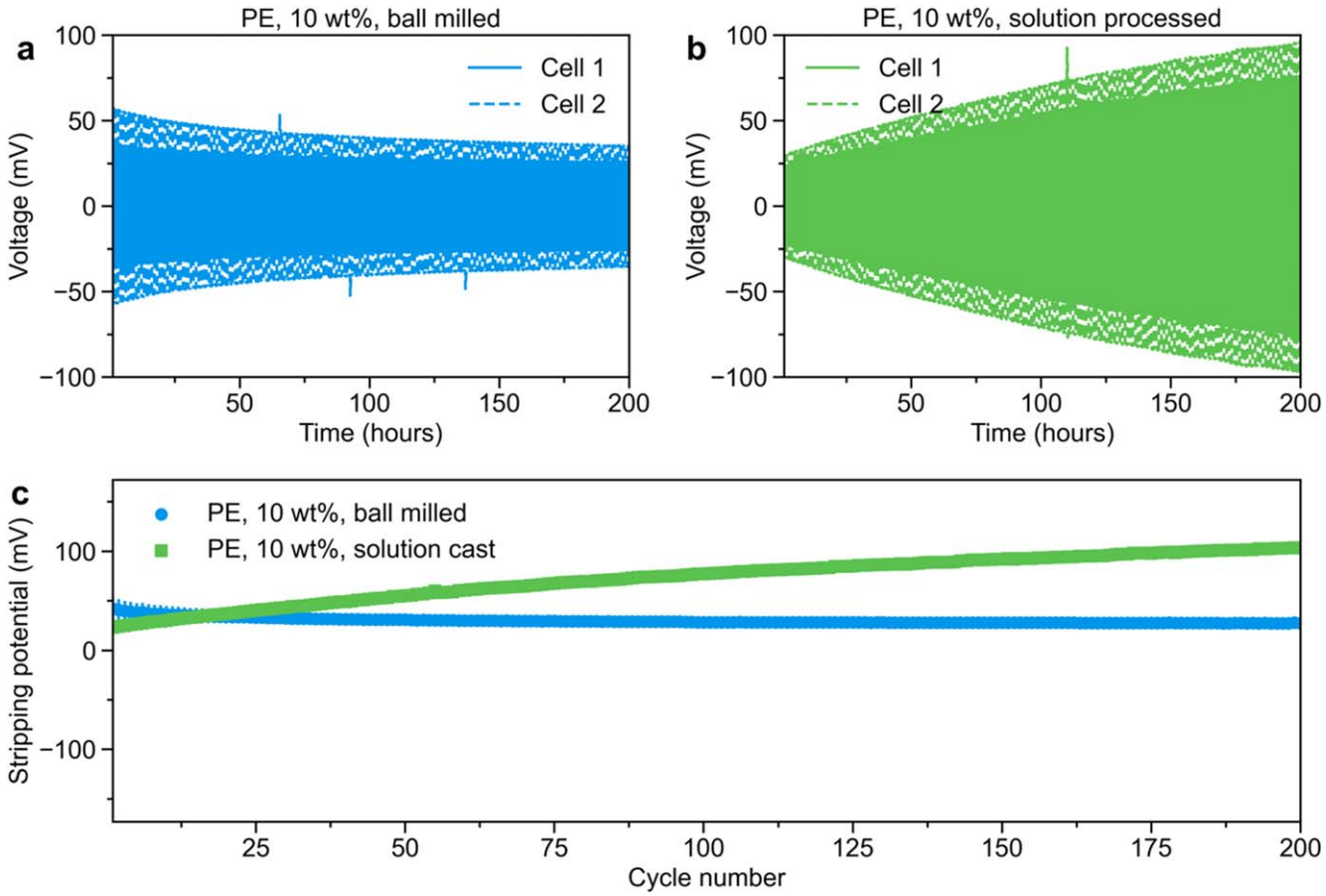

Figure 4. Long-term cycling performance with Li-metal. Li || Li cycling performance of (a) ball milled PE, 10 wt% and (b) solution processed, PE-LPS, 10 wt%. Average Li stripping overpotential of (c) both ball milled and solution processed PE hybrids. All cycling was conducted at 60 °C and the current density used was 0.05 mA cm^{-2} to a capacity of 0.05 mAh cm^{-2}. Ball milled data in subfigures (a) and (c) were reproduced with permission from *ACS Appl. Energy Mater.* 2022, *5* (7), 8900–8912.

Our previous work demonstrated that ball milled LPS did not last more than 500 h (250 cycles),[12] while the ball milled polymer hybrids were able to cycle for 1000 h (500 cycles). This observation holds for the solution processed, 10 wt% PE sample (Fig. S7), and both ball milled and solution processed samples could cycle for twice as long as the pristine LPS. This is striking because the solution processed 10 wt% PE sample is the least conductive of all samples discussed in this paper. In our previous work, we suggested that the longer cycle life in the polymer hybrids was due to an improvement in the mechanical properties of the LPS because of the addition of polymer.[12,47] The resulting hybrid pellets were thinner (∼0.2 mm) than the pristine sulfide (∼1 mm) and were less prone to fracturing after cold pressing (100 mbar), demonstrating that the inclusion of polymer improves the mechanical properties. Additionally, the observation that the highly conductive, pristine sulfide cannot cycle as long as a polymer hybrid with much lower conductivity suggests that conductivity does not solely govern the long-term cycling behavior of sulfide systems.[47–49]

Although both ball milled and solution processed hybrid samples had similar cycle life, the main difference between these two systems appears to be the overpotential as a function of time. Figure 4c tracks the overpotential for lithium stripping as a function of cycle number for the first 200 cycles. The overpotentials shown in Fig. 4c are the average of 3 separate cells. From this figure, we can clearly see that the overpotential of the first 20 cycles stays the same between the ball milled (∼45 mV) and the solution processed (∼50 mV) PE hybrids. However, after cycle 20, the overpotential of the ball milled hybrid stays roughly the same until cycle 200 (∼30 mV), whereas the overpotential of the solution processed hybrid steadily increases to 100 mV, eventually increasing to 150 mV by cycle 500 (Fig. S7). While it is true that the solution processed PE hybrid has much lower conductivity than its ball milled counterpart, both hybrids began cycling with roughly the same overpotential. Therefore, this steady increase in overpotential cannot be attributed to conductivity alone.

We suspect that this could be due to the distribution of the PE within the LPS. It has been widely reported in the literature that sulfide-type electrolytes form cracks and voids during lithium plating and stripping,[49,50] which is the main mechanism for cell failure. In situ studies have also shown that during cycling, these cracks increase in size over time,[51] providing an easy space for lithium dendrites to grow and eventually cause cell death.[52] We anticipate that in a PE hybrid, the cracks that develop during cycling are filled by polymer, and that as the cracks expand over time, the polymer may "creep" into the cracks. These samples are cycled at 60 °C, below the melt transition for polyethylene, but still much higher than the glass transition of this polymer,[53] which lends credence to the possibility that the polymer may be able to fill the expanding cracks during LPS cycling. Figure 2 demonstrated that the solution processed PE-LPS sample shows more surface-area coverage by the polymer than the ball milled sample. Therefore, during cycling, there will be PE throughout the whole electrolyte, rather than it being localized into one area. Because PE is an insulating polymer and ions cannot pass through it, over time the overpotential of lithium stripping will increase as the polymer fills the LPS cracks and physically separate the LPS particles.

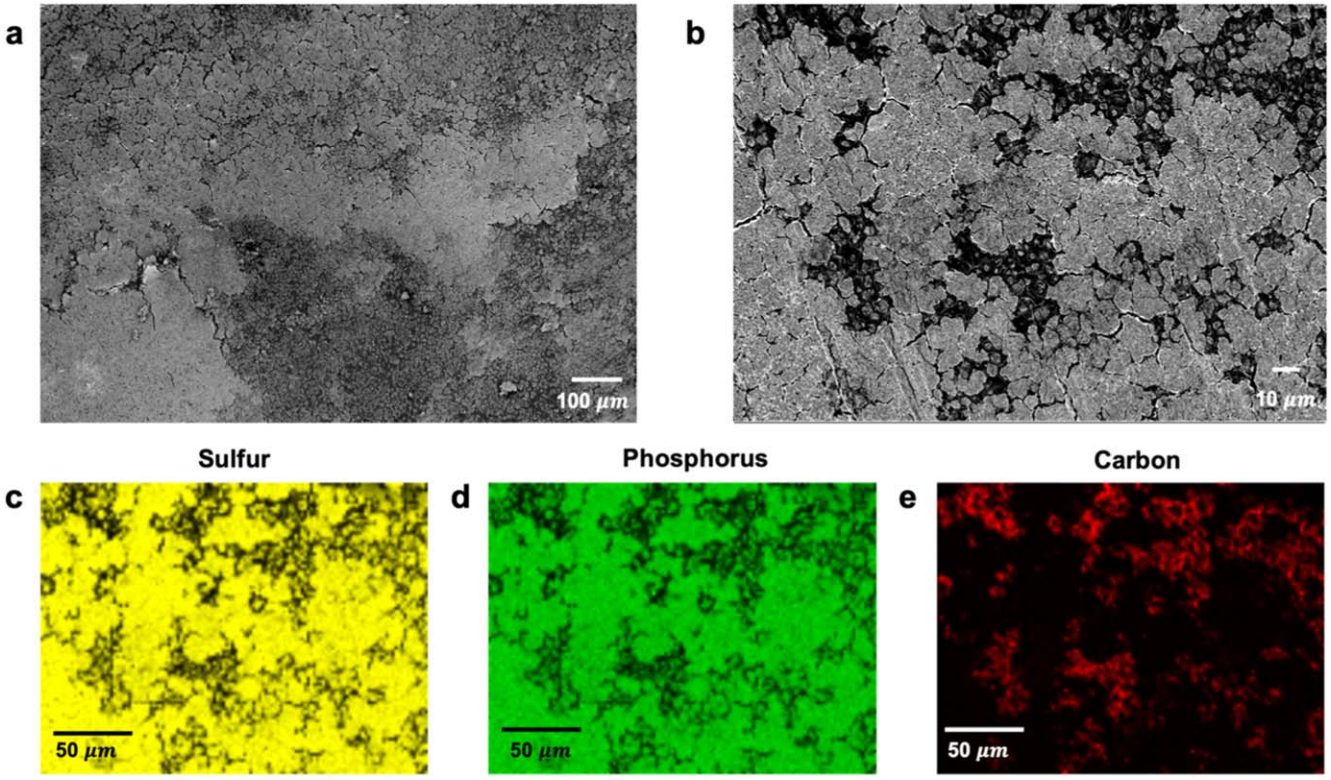

Figure 5. Understanding surface morphology after Li-metal cycling. (a), (b) SEM images of a solution processed, 10 wt% PE electrolyte show large polymer surface coverage. Energy-dispersive X-ray spectroscopy (EDS) images show the (c) sulfur, (d) phosphorus, and (e) carbon elemental distributions.

Understanding polymer-inorganic morphology in solution processed hybrids after cycling.—To investigate whether the PE can "creep" into the cracks and voids formed in LPS during cycling, post-mortem SEM images were taken of solution processed PE-LPS hybrids that had been cycled in a symmetric Li ‖ Li half cell. Cell 1 from Fig. 4b was decrimped and the lithium metal electrodes were removed from the pellet. Figure 5 shows the resulting SEM with energy-dispersive X-ray spectroscopy (EDS) images of cell 1 after cycling for approximately 1000 h (500 cycles). It is clear to see that the polymer continues to have a high level of surface coverage of the pellet (Fig. 5a). However, unlike the pre-cycled sample (Fig. 2d), there seems to be more polymer in the cracks of the LPS. It appears as if the polymer is not only "creeping" further into the volume of the cracks, but also horizontally across the pellet surface, implying that during cycling, the polymer is not stationary, and moves throughout the inorganic. Figure 5b shows a higher magnification image of the same area of the pellet as Fig. 5a, and this clearly shows that the polymer is filling the cracks of the LPS. To fully demonstrate that our assignment of the black regions as PE is correct, EDS spot spectra (Fig. S8) were taken at two sites on the region shown in Fig. 5b. Spectrum 1 was obtained from the light grey area, which we assigned to LPS, and the resulting elemental distribution shows a large intensity for sulfur and phosphorus. Contrastingly, the amount of carbon in this area is minimal, further demonstrating that the light grey regions are the inorganic LPS. Additionally, spectrum 2 was taken in one of the black areas, and the results show a large peak for carbon, greater than any of the other elements (sulfur or phosphorus) probed, confirming this area as PE. Because of the SEM instrument limitations, quantifying carbon is difficult, and only qualitative comparisons can be made when analyzing these spot spectra.

To conclusively delineate the inorganic and polymeric regions, sulfur (Fig. 5c), phosphorus (Fig. 5d), and carbon (Fig. 5e) elemental mapping (EDS) was performed. The carbon mapping shows that the polymer is well dispersed within the inorganic, corroborating the observations that we made in the pre-cycling SEM (Fig. 2) and EDS (Fig. S3) analyses of the solution processed hybrids. Interestingly, the post-cycling EDS mapping demonstrates that there are small regions of the inorganic within the polymer, implying that during cycling, the polymer continues to separate the inorganic grains over time. To show this phenomenon clearly, higher magnification SEM images of this electrolyte were taken (Fig. S9). These high magnification images show the creep behavior of the polymer as well as the LPS "islands" that form within the polymer matrix. During cycling, the polymer appears to creep into the cracks of the LPS, which causes a mechanically stabilizing effect and allows for longer cycle life in comparison to the pristine inorganic. However, this creep behavior does have a drawback in that the insulating polymer blocks pathways for ion conduction through the LPS, leading to a steadily increasing overpotential over time.

We expect the same behavior of the polymer filling the LPS cracks to occur in the ball milled sample. By contrast, because of the random, granular distribution of the PE in the ball milled sample, we anticipate that this effect is less pronounced. Because the PE is localized to certain areas in the hybrid pellet, the ion transport pathways remain continuous through the LPS, and therefore ion conduction is not significantly hampered. This would result in a stable, steady overpotential for lithium stripping and deposition over time, as observed in Fig. 4. In-situ imaging (such as tomography) of these hybrid electrolytes can lead to a greater understanding of the polymer creep behavior during cycling, and the relationship between hybrid mechanical properties and electrochemical behavior will be performed in future studies.

Conclusions

In conclusion, the effect of processing methodology on the performance of composite sulfide-polymer solid state electrolytes was investigated. Li_3PS_4-polymer hybrids were prepared using polyethylene as the polymer component and fabricated either via ball-milling or solution processing in toluene. We demonstrated that the two methods led to a different polymer-inorganic microstructure with

the solution processed hybrids exhibiting a more homogenous distribution of the polymer within the inorganic as well as an active separation of inorganic particles unlike the ball milled hybrids. We then showed that the differences in distribution had large effects on the overall conductivity, with the solution processed hybrids having a much lower conductivity than the ball milled hybrids. Additionally, we found that processing LPS in toluene introduces a small degree of crystallinity despite the relative non-polarity of the solvent. Finally, we investigated the impact of solution processing and ball milling on the overall cycling performance of these electrolytes with Li-metal. We found that the solution processed electrolytes exhibited a consistent increase in overpotential for lithium stripping and deposition over time whereas ball milled samples displayed a steady overpotential. Post-cycling SEM and EDS analysis of the solution processed polymer hybrid revealed that the homogenous polymer distribution and creep behavior are likely responsible for the differences in overpotential between the solution processed and ball milled hybrids. Our work provides a deeper understanding of how processing methodology affects the microstructure of hybrid sulfide-polymer electrolytes and the resulting impact on the overall electrochemical behavior. The insights generated from our work can further inform the development of hybrid electrolytes, directing focus towards generating synthetic procedures that are scalable but do not compromise on electrolyte performance.

Experimental

Materials and electrolyte synthesis.— *Materials.*—Li_2S was purchased form MSE Supplies (99%). P_2S_5 (99%) was purchased from Sigma-Aldrich. Both Li_2S and P_2S_5 were stored in an Argon-filled glovebox (Vigor Tech, H_2O and $O_2 < 1$ ppm) solely dedicated to sulfide work. Ball milling balls (5 mm) made of Yttria-stabilized ZrO_2 (YSZ) were purchased from MSE Supplies. Lithium metal (0.75 mm, 99.9% metals basis) and Indium ingot (99.999%) were purchased from Alfa Aesar.

Polyethylene (3.5×10^4 g mol^{-1}) and poly(ethylene oxide) (1×10^5) were purchased from Sigma-Aldrich. Prior to use, polymers were vacuum dried at 50 °C overnight before being transferred to an Argon-filled glovebox.

Synthesis of LPS.—Amorphous Li_3PS_4 was synthesized using a 3:1 mol ratio of Li_2S and P_2S_5 according to our previously published procedure.[29] To confirm LPS purity, ^{7}Li solid-state nuclear magnetic resonance (NMR) spectroscopy (Bruker, Wide-bore, 400 MHz, etc) was performed.

Ball milling of hybrid electrolytes.—A Retsch PM-100 ball mill was used for all experiments. A 45 ml ZrO_2 jar (Retsch) with a screw-top clamp for sealing was used for ball milling. All sample preparation was performed in an Argon-filled glovebox. Ball milled samples were synthesized according to our previous published procedure.[12] Samples were prepared in 0.5 g batches, and approximately 8 g of 5 mm zirconia balls were added to the jar. The hybrids were ball milled at a speed of 450 rpm for 10 h with frequent rest steps every 5 min to prevent overheating of the polymer.

Solution processing of hybrid electrolytes.—Solution processed hybrid electrolytes and solution processed LPS were synthesized in 0.5 g batches. Ball milled LPS was weighed in an Argon-filled glovebox and added to a 20 ml glass vial, then 5 ml toluene (dried overnight with 4 Å molecular sieves from Sigma) was added (in a 100 mg ml^{-1} ratio). A stir bar was added to the vial and the LPS and toluene were stirred at medium speed for 5 min. Next, the appropriate mass of PEO or PE was then added carefully to the suspension. When preparing PEO-LPS hybrids, this mixture was left to stir overnight at ambient glovebox temperature with the cap on. Next, it was left overnight to stir at 60 °C, uncapped to let excess toluene evaporate. Samples were then vacuum-dried at 60 °C and 100 mbar to evaporate remaining toluene. When preparing PE-LPS hybrids, the initial mixture was left to stir overnight with the cap on at the raised temperature of 90 °C to allow the PE to dissolve in the toluene. Next, it was left overnight to stir at 90 °C uncapped to let excess toluene evaporate. Finally, samples were vacuum-dried overnight at 90 °C and 100 mbar to evaporate remaining toluene. Solution processed LPS was prepared according to the same procedure for PE-LPS but using ball milled LPS as the precursor without the addition of polymer. ^{1}H solution state NMR spectroscopy (Bruker, 400 MHz, narrow-bore) was used to confirm the removal of toluene (Fig. S1).

Sample characterization.— *SEM imaging.*—Samples for SEM were prepared by securing pellets onto stainless-steel mounts (TedPella) with Cu tape. Approximately 100 mg of sample powder loaded into a pellet chamber with a 10 mm diameter (MTI Corporation, DIE10B), and a piston was placed inside the chamber. The chamber was then placed into a 15 T hydraulic press (MTI Corporation, YLJ-15L) and pressed at a pressure of 100 bar (10 MPa) for about one minute. All images were taken on a Carl Zeiss Merlin Field Emission Scanning Electron Microscope at ambient temperature. Electron dispersive X-ray spectroscopy (EDS) measurements were performed in the Carl Zeiss Merlin Field Emission Scanning Electron Microscope using an Oxford UltimMax100 EDS system. EDS samples were coated with 5 nm Pt/Pd using a Cressington 208 HR sputter coater before testing. EDS spectra and mapping images were collected under 10 kV accelerating voltage and 256 pA current.

DSC measurements.—Approximately 5 mg of samples were placed inside an Al Tzero Pan with a hermetic lid (TA Instruments) and sealed inside an Argon filled glovebox (O_2, $H_2O < 1$ ppm) with a crimper (TA Instruments). Measurements were conducted on a TA Instruments Discovery 2500 Differential Scanning Calorimeter. Scans were conducted between −90 °C to 250 °C at a rate of 10 °C min^{-1}, with the first scan starting at 30 °C. Three scans were taken per sample. Peaks were integrated by first isolating the area where the peaks occurred in each sample, making this region all non-negative by adding the lowest y value to the entire graph, and lastly using the scipy.integrate.simps python function to find the absolute value of the area under the curve using Simpson's rule.[54]

Solid state magic angle spinning (MAS) NMR spectroscopy.—Solid state spectra were collected on a Bruker Avance III 400 MHz wide-bore magnet under a field of 9.5 T with a standard solids broadband probe. Approximately 10–15 mg of sample were packed into a 1.9 mm ZrO_2 rotor with polyimide caps (Cortec Net) inside an Ar filled glovebox. Rotors were spun at a rate of 20 KHz, and ^{7}Li spectra were acquired using a 90° pulse time of 0.9 μ s at a power of 90 W. Recycle delay times varied from 20 s for pristine LPS to 20–40 s for the ball milled and solution cast hybrids. Receiver gain was performed automatically, and the intensity of all spectra were normalized to receiver gain and sample mass. A total of 16 scans were collected for each spectrum. The ^{7}Li chemical shift was referenced to LiF at −1.0 ppm (reference frequency of −378.24 Hz).

XRD measurements.—Approximately 50 mg of samples were placed on a polyimide substrate and the samples were covered by a kapton tape (thickness of 25 μm) inside an Argon-filled glovebox. X-ray diffraction measurements were conducted using the Rigaku SmartLab X-ray diffractometer equipped with a HyPix3000 detector. The instrument employed Cu Kα radiation with a wavelength of 1.54186 Å. Scans were conducted in a parallel beam mode with the Cross Beam Optics attachment. The X-ray tube was operated at 44 mA and 40 kV. Data collection and analysis were performed using the SmartLab Studio II software package, version 4.4.241.0.

Electrochemical characterization.— *Coin cell fabrication.*—Coin cell (CR 2032) parts were purchased from Xiamen TOB New Energy Technology. All sample preparation was performed in

an Argon-filled glovebox. Approximately 30–40 mg of hybrid sample powder (both solution cast and ball milled) or 100–120 mg of LPS powder was loaded into a pellet chamber with a 10 mm diameter. The chamber was then placed into a 15 T hydraulic press (MTI Corporation, YLJ-15L) and pressed at a pressure of 100 bar (10 MPa) for about 1 min to form a pellet. Pellet thicknesses ranged from approximately 0.3–0.4 mm for the hybrids and 0.8–1 mm for LPS. Indium or lithium foils were rolled into 0.25 mm thick strips and cut into electrodes with 6 mm diameters. Coin cells were then crimped at a pressure of 650 kg.

Electrochemical impedance spectroscopy.—Impedance measurements were taken using a BioLogic VSP-300 potentiostat with a frequency range of 7 MHz to 1 Hz in an ESPEC environmental chamber. Samples were assembled into coin cells using indium blocking electrodes with a thickness of 0.25 mm and a diameter of 6 mm. Sample were heated to 120 °C and then cooled, in 10-degree intervals, back to 20 °C, with a 45-minute equilibration step at each temperature. After impedance runs were completed, coin cells were de-crimped and the thickness of the pellet was measured and used to calculate conductivity.

Symmetric Li||Li cycling.—Symmetric Li||Li cycling measurements were taken using a Neware BTS4000 battery tester. Samples were allowed to rest for 10 h at 60 °C before cycling. Cutoff voltages were set to be 1 V and −2V vs Li/Li^+.

Acknowledgments

This work was partially supported by the University of Chicago Materials Research Science and Engineering Center (MRSEC), which is funded by the National Science Foundation under award number DMR-2011854. Parts of this work (DSC) were carried out at the Soft Matter Characterization Facility of the University of Chicago. Solution state NMR measurements were taken at the UChicago Chemistry NMR facility. Solid state NMR experiments were performed at the University of Illinois at Chicago NMR facility (NIH award 1S10RR025105–01). The authors thank Daniel McElheny for help in setting up some of the solid state NMR parameters. C.F. and Z.U. acknowledge support from the UChicago Jeff Metcalf Internship Program. E.S.D. acknowledges the NSF NRT AIMEMS Fellowship. P. Mirmira wishes to acknowledge Anjali Mirmira for fruitful discussions.

ORCID

Priyadarshini Mirmira https://orcid.org/0000-0002-3004-7227
Peiyuan Ma https://orcid.org/0000-0003-0373-3712
Chibueze V. Amanchukwu https://orcid.org/0000-0002-6573-1213

References

1. J.-M. Tarascon and M. Armand, "Issues and challenges facing rechargeable lithium batteries." *Nature*, **441**, 359 (2001).
2. C. V. Amanchukwu, "The electrolyte frontier: a manifesto." *Joule*, **4**, 281 (2020).
3. M. Keller, A. Varzi, and S. Passerini, "Hybrid electrolytes for lithium metal batteries." *J. Power Sources*, **392**, 206 (2018).
4. C.-F. Li, R. Muruganantham, W.-C. Hsu, M. Ihrig, C.-T. Hsieh, C.-C. Wang, and W.-R. Liu, "Atomic layer deposition of ZnO on Li1.3Al0.3Ti1.7(PO4)3 enables its application in all solid-state lithium batteries." *J. Taiwan Inst. Chem. Eng.*, **144**, 104681 (2023).
5. R. Muruganantham, C.-Y. Lin, H.-W. Wu, D. H. Gregory, and W.-R. Liu, "Interface design strategy in combined materials of lithium thiophosphate electrolyte for solid-state lithium-ion batteries applications." *J. Taiwan Inst. Chem. Eng.*, **138**, 104446 (2022).
6. R. Guo et al., "Interfacial challenges and strategies toward practical sulfide-based solid-state lithium batteries." *Energy Mater. Adv.*, **4**, 0022 (2023).
7. C. A. Angell, "Polymer electrolytes—some principles, cautions, and new practices." *Electrochim. Acta*, **250**, 368 (2017).
8. K. Zhang et al., "8.5 Mm-thick flexible-rigid hybrid solid–electrolyte/lithium integration for air-stable and interface-compatible all-solid-state lithium metal batteries." *Adv. Energy Mater.*, **12**, 2200368 (2022).
9. J. Zheng, P. Wang, H. Liu, and Y. Y. Hu, "Interface-enabled ion conduction in Li10GeP2S12-Poly(Ethylene Oxide) hybrid electrolytes." *ACS Appl. Energy Mater.*, **2**, 1452 (2019).
10. F. J. Simon, M. Hanauer, F. H. Richter, and J. Janek, "Interphase formation of PEO20:LiTFSI-Li6PS5Cl composite electrolytes with lithium metal." *ACS Appl. Mater. Interfaces*, **12**, 11713 (2020).
11. M. Li, M. Kolek, J. E. Frerichs, W. Sun, X. Hou, M. R. Hansen, M. Winter, and P. Bieker, "Investigation of polymer/ceramic composite solid electrolyte system: the case of PEO/LGPS composite electrolytes." *ACS Sustain. Chem. Eng.*, **9**, 11314 (2021).
12. P. Mirmira, C. Fuschi, W. Gillett, P. Ma, J. Zheng, Z. Hood, and C. Amanchukwu, "Nonconductive polymers enable higher ionic conductivities and suppress reactivity in hybrid sulfide–polymer solid state electrolytes." *ACS Appl. Energy Mater.*, **5**, 8900 (2022).
13. F. J. Simon, M. Hanauer, A. Henss, F. H. Richter, and J. Janek, "Properties of the interphase formed between argyrodite-type Li6PS5Cl and polymer-based PEO10: LiTFSI." *ACS Appl. Mater. Amp Interfaces*, **11**, 42186 (2019).
14. D. H. S. Tan et al., "Enabling thin and flexible solid-state composite electrolytes by the scalable solution process." *ACS Appl. Energy Mater.*, **2**, 6542 (2019).
15. K. Lee, S. Kim, J. Park, S. H. Park, A. Coskun, D. S. Jung, W. Cho, and J. W. Choi, "Selection of binder and solvent for solution-processed all-solid-state battery." *J. Electrochem. Soc.*, **164**, A2075 (2017).
16. M. Ghidiu, J. Ruhl, S. P. Culver, and W. G. Zeier, "Solution-based synthesis of lithium thiophosphate superionic conductors for solid-state batteries: a chemistry perspective." *J. Mater. Chem. A*, **7**, 17735 (2019).
17. E. C. Self, Z. D. Hood, T. Brahmbhatt, F. M. Delnick, H. M. Meyer, G. Yang, J. L. M. Rupp, and J. Nanda, "Solvent-mediated synthesis of amorphous Li3PS4/Polyethylene oxide composite solid electrolytes with high Li+ conductivity." *Chem. Mater.*, **32**, 8789 (2020).
18. Y. Zhao, C. Wu, G. Peng, X. Chen, X. Yao, Y. Bai, F. Wu, S. Chen, and X. Xu, "A new solid polymer electrolyte incorporating Li10GeP2S12 into a polyethylene oxide matrix for all-solid-state lithium batteries." *J. Power Sources*, **301**, 47 (2016).
19. L. Chen, Y. Li, S.-P. Li, L.-Z. Fan, C.-W. Nan, and J. B. Goodenough, "PEO/garnet composite electrolytes for solid-state lithium batteries: from 'Ceramic-in-Polymer' to 'Polymer-in-Ceramic." *Nano Energy*, **46**, 176 (2018).
20. T. Inada, K. Takada, A. Kajiyama, M. Kouguchi, H. Sasaki, S. Kondo, M. Watanabe, M. Murayama, and R. Kanno, "Fabrications and properties of composite solid-state electrolytes." *Solid State Ion*, **158**, 275 (2003).
21. F. Wu, K. Zhang, Y. Liu, H. Gao, Y. Bai, X. Wang, and C. Wu, "Polymer electrolytes and interfaces toward solid-state batteries: recent advances and prospects." *Energy Storage Mater.*, **33**, 26 (2020).
22. K. Yamamoto et al., "High ionic conductivity of liquid-phase-synthesized Li 3 PS 4 solid electrolyte, comparable to that obtained via ball milling." *ACS Appl. Energy Mater.*, **4**, 2275 (2021).
23. M. B. Dixit et al., "Nanoscale mapping of extrinsic interfaces in hybrid solid electrolytes." *Joule*, **4**, 207 (2020).
24. A. Hayashi, T. Harayama, F. Mizuno, and M. Tatsumisago, "Mechanochemical synthesis of hybrid electrolytes from the Li2S–P2S5 glasses and polyethers." *J. Power Sources*, **163**, 289 (2006).
25. I. Villaluenga, K. H. Wujcik, W. Tong, D. Devaux, D. H. C. Wong, J. M. DeSimone, and N. P. Balsara, "Compliant glass–polymer hybrid single ion-conducting electrolytes for lithium batteries." *Proc. Natl Acad. Sci.*, **113**, 52 (2016).
26. The Materials Project, "Materials Data on Li3PS4." *Materials Project* (2020).
27. N. Riphaus, P. Strobl, B. Stiaszny, T. Zinkevich, M. Yavuz, J. Schnell, S. Indris, H. A. Gasteiger, and S. J. Sedlmaier, "Slurry-based processing of solid electrolytes: a comparative binder study." *J. Electrochem. Soc.*, **165**, A3993 (2018).
28. H. Stöffler et al., "Li+-Ion dynamics in β-Li3PS4 observed by NMR: local hopping and long-range transport." *J. Phys. Chem. C*, **122**, 15954 (2018).
29. P. Mirmira, J. Zheng, P. Ma, and C. Amanchukwu, "Importance of multimodal characterization and influence of residual Li2S impurity in amorphous Li3PS4 inorganic electrolytes." *J. Mater. Chem. A*, **9**, 19637 (2021).
30. Z. Liu, W. Fu, E. A. Payzant, X. Yu, Z. Wu, N. J. Dudney, J. Kiggans, K. Hong, A. J. Rondinone, and C. Liang, "Anomalous high ionic conductivity of nanoporous β-Li 3PS4." *J. Am. Chem. Soc.*, **135**, 975 (2013).
31. C. Dietrich, D. A. Weber, S. J. Sedlmaier, S. Indris, S. P. Culver, D. Walter, J. Janek, and W. G. Zeier, "Lithium ion conductivity in Li2S-P2S5 glasses-building units and local structure evolution during the crystallization of superionic conductors Li3PS4, Li7P3S11 and Li4P2S7." *J. Mater. Chem. A*, **5**, 18111 (2017).
32. H. Tsukasaki, Y. Mori, M. Otoyama, S. Yubuchi, T. Asano, Y. Tanaka, T. Ohno, S. Mori, A. Hayashi, and M. Tatsumisago, "Crystallization behavior of the Li2S-P2S5 glass electrolyte in the LiNi1/3Mn1/3Co1/3O2 positive electrode layer." *Sci. Rep.*, **8**, 6214 (2018).
33. H. Tsukasaki, H. Morimoto, and S. Mori, "Thermal behavior and microstructure of the Li3PS4–ZnO composite electrolyte." *J. Power Sources*, **436**, 226865 (2019).
34. T. Yersak, J. R. Salvador, R. D. Schmidt, and M. Cai, "Hot pressed, fiber-reinforced (Li2S)70(P2S5)30 solid-state electrolyte separators for Li metal batteries." *ACS Appl. Energy Mater.*, **2**, 3523 (2019).
35. Ö. U. Kudu et al., "Structural details in Li3PS4: variety in thiophosphate building blocks and correlation to ion transport." *Energy Storage Mater.*, **44**, 168 (2022).
36. J. Gao, Y.-S. S. Zhao, S.-Q. Q. Shi, and H. Li, "Lithium-ion transport in inorganic solid state electrolyte." *Chinese Physics B*, **25**, 018211 (2015).
37. F. N. Forrester, J. A. Quirk, T. Famprikis, and J. A. Dawson, "Disentangling cation and anion dynamics in Li3PS4Solid electrolytes." *Chem. Mater.*, **34**, 10561 (2022).
38. Z. D. Hood, H. Wang, Y. Li, A. S. Pandian, M. Parans Paranthaman, and C. Liang, "The 'Filler Effect': a study of solid oxide fillers with β-Li3PS4 for lithium conducting electrolytes." *Solid State Ion*, **283**, 75 (2015).
39. A. Gries, F. Langer, J. Schwenzel, and M. Busse, "Determination of reaction enthalpies of synthesizing β-Li3PS4 in tetrahydrofuran." *ACS Omega*, **8**, 14034 (2023).

40. H. Stöffler et al., "Amorphous versus crystalline Li3PS4: local structural changes during synthesis and Li Ion mobility." *J. Phys. Chem. C*, **123**, 10280 (2019).
41. S. Wang et al., "High-conductivity free-standing Li6PS5Cl/Poly(Vinylidene Difluoride) composite solid electrolyte membranes for lithium-ion batteries." *J. Materiomics*, **6**, 70 (2020).
42. G. Liu, H. Zheng, X. Song, and V. S. Battaglia, "Particles and polymer binder interaction: a controlling factor in lithium-ion electrode performance." *J. Electrochem. Soc.*, **159**, A214 (2012).
43. R. Fang, H. Xu, B. Xu, X. Li, Y. Li, and J. B. Goodenough, "Reaction mechanism optimization of solid-state Li–S batteries with a PEO-based electrolyte." *Adv. Funct. Mater.*, **31**, 2001812 (2021).
44. J. Zheng and Y.-Y. Hu, "New insights into the compositional dependence of Li-Ion transport in polymer–ceramic composite electrolytes." *ACS Appl. Mater. Interfaces*, **10**, 4113 (2018).
45. J. Zheng, M. Tang, and Y.-Y. Hu, "Lithium ion pathway within Li7La3Zr2O12 -polyethylene oxide composite electrolytes." *Angew. Chem.*, **128**, 12726 (2016).
46. J. C. Bachman et al., "Inorganic solid-state electrolytes for lithium batteries: mechanisms and properties governing ion conduction." *Chem. Rev.*, **116**, 140 (2016).
47. Y. Ren, N. Hortance, and K. B. Hatzell, "Mitigating chemo-mechanical failure in Li-S solid state batteries with compliant cathodes." *J. Electrochem. Soc.*, **169**, 060503 (2022).
48. Y. S. Oh, M. Kim, S. Kang, J.-Y. Park, and H.-T. Lim, "Redox activity of Li2S–P2S5 electrolyte inducing chemo-mechanical failure in all-solid-state batteries comprising sulfur composite cathode and Li–Si alloy anode." *Chem. Eng. J.*, **442**, 136229 (2022).
49. M. B. Dixit, N. Singh, J. P. Horwath, P. D. Shevchenko, M. Jones, E. A. Stach, T. S. Arthur, and K. B. Hatzell, "In situ investigation of chemomechanical effects in thiophosphate solid electrolytes." *Matter*, **3**, 2138 (2020).
50. L. L. Baranowski, C. M. Heveran, V. L. Ferguson, and C. R. Stoldt, "Multi-scale mechanical behavior of the Li3PS4 solid-phase electrolyte." *ACS Appl. Mater. Interfaces*, **8**, 29573 (2016).
51. N. Seitzman, H. Guthrey, D. B. Sulas, H. A. S. Platt, M. Al-Jassim, and S. Pylypenko, "Toward all-solid-state lithium batteries: three-dimensional visualization of lithium migration in β-Li 3 PS 4 ceramic electrolyte." *J. Electrochem. Soc.*, **165**, A3732 (2018).
52. J. H. Cho, K. Kim, S. Chakravarthy, X. Xiao, J. L. M. Rupp, and B. W. Sheldon, "An investigation of chemo-mechanical phenomena and li metal penetration in all-solid-state lithium metal batteries using in situ optical curvature measurements." *Adv. Energy Mater.*, **12**, 2200369 (2022).
53. F. C. Stehling and L. Mandelkern, "The glass temperature of linear polyethylene." *Macromolecules*, **3**, 242 (1970).
54. P. Virtanen et al., "SciPy 1.0: fundamental algorithms for scientific computing in python." *Nat. Methods*, **17**, 261 (2020).